RESEARCH ARTICLE - SOLID EARTH SCIENCES

Fault modelling, seismic sequence evolution and stress transfer scenarios for the July 20, 2017 (M_W 6.6) Kos–Gökova Gulf earthquake, SE Aegean

Sotirios Sboras[1] · Ilias Lazos[2] · Evaggelos Mouzakiotis[1] · Vassilios Karastathis[1] · Spyros Pavlides[2] · Alexandros Chatzipetros[2]

Abstract

The July 20, 2017, M_W 6.6 Kos–Gökova Gulf earthquake occurred offshore, near Bodrum of Turkey and Kos of Greece. It was one of the strongest in the broader area during the last many decades causing two deaths, many injuries and extensive damages. We investigated the evolution of the seismic sequence using seismological and geological tools. The aftershock sequence was relocated mainly in order to define the geometry of the main seismic source, depicting a NNW-dipping fault plane. It also revealed significant clustering, associated with other nearby faults, and asymmetric spatio-temporal evolution. Along with morphotectonic analysis on Kos Island, and other published seismological information (e.g. focal mechanisms), we modelled the seismic source of the mainshock, as well as the one of the strongest aftershocks (August 8, M_W 5.3). We applied the Coulomb failure criterion in order to investigate the effect of the mainshock on the strongest aftershock, and the rest of the sequence as well. Using the same method, we also investigated the stress changes of both strongest shocks for the prevailing E–W-trending normal faults in this area. Among other conclusions and implications, we deduce that the prevailing tectonic setting of the Gökova Gulf consists of roughly E–W-striking normal faults forming inner horsts and grabens.

Keywords Kos–Gökova earthquake sequence · Epicentral relocation · Coulomb stress change · Seismotectonics · SE Aegean

Introduction

On July 20, 2017, at 22:31:11.0 (UTC), a strong (M_W 6.6) and destructive earthquake occurred in the southeastern Aegean Sea, near the border region of Greece and Turkey. The epicentre is located offshore, within the Gökova (Keramikos) Gulf, between Kos Island in Greece and Bodrum City in Turkey, at an initially calculated depth of 10.2 km (NOA). The earthquake caused two deaths and 120 injuries on Kos Island; only historic monuments in Kos town suffered extensive damage (IESEE 2017; Psycharis and Taflampas 2017; Kiratzi and Koskosidi 2018). In Bodrum

area, 90 people were injured, 26 buildings collapsed, and 941 buildings were damaged, 202 of which heavily (Alcik 2018). The mainshock was preceded 21 min before by a M_L 2.9 foreshock near to the mainshock's epicentre and was followed by numerous aftershocks, the strongest of which (M_W 5.3) was recorded many days later, on August 8, 18 km east of Bodrum.

The broader Kos–Gökova Gulf region demonstrates quite intense historical seismicity (Fig. 1). The oldest recorded event occurred in 412 BC (Ambraseys and White 1997; Papazachos and Papazachou 2003), with estimated magnitude and intensity M 6.8 and IX MM, respectively, near the mid-southern coast of Kos Island (Papazachos and Papazachou 2003). The strongest event occurred during the early instrumental period, on June 26, 1926, with a magnitude of M 7.6 and intensity of XI MM. Its epicentral location is estimated ca. 45 km SE of Kos Island and its hypocentral depth at 100 km (Papazachos and Papazachou 2003). During the instrumental period, a strong M_L 6.1 (V + MM, according to Papazachos and Papazachou 2003) earthquake occurred on

✉ Ilias Lazos
 iliaslazoseng@yahoo.com

1 Institute of Geodynamics, National Observatory of Athens, Athens, Greece

2 Department of Geology, Aristotle University of Thessaloniki, Thessaloniki, Greece
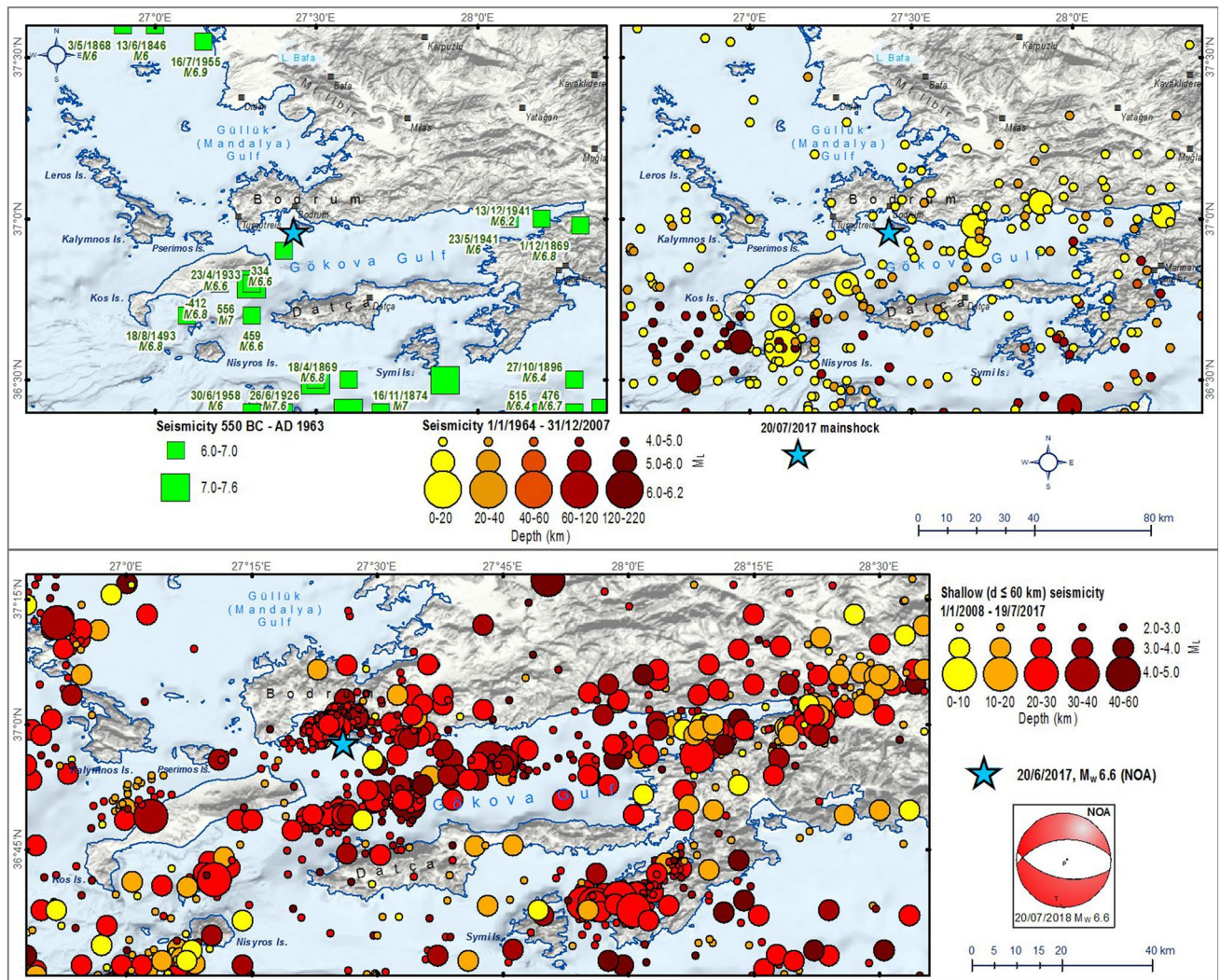
Fig. 1 Seismicity of the broader Kos–Gökova Gulf area for different periods. (*Top left*) Historic and early instrumental period (550 BC–AD 1963) for $M \geq 6.0$ events (Papazachos and Papazachou 2003). (*Top right*) Recent instrumental period (1964–2007) for $M_L \geq 4.0$ events (IG–NOA's catalogue). (*Bottom*) Very recent instrumental period (2008–19/7/2017) only for shallow earthquakes ($d \leq 60$ km) with $M_L \geq 2.0$ (IG–NOA's catalogue); IG–NOA's moment tensor solution of the 20/7/2017 mainshock is also shown

December 5, 1968, just west of Nisyros Island at a depth of 10 km, while many events between M_L 5.0 and M_L 6.0 have been recorded within this region (Fig. 1).

Static stress transfer not only can help us to understand the conditions under which the aftershock sequence evolved, but to give us a degree of validation for our fault model(s). As already shown in other significant seismic events, aftershocks and subsequent main shocks often occur in regions of increased Coulomb stress caused by the main shock, while earthquakes become less prevalent than before the main shock in regions subject to Coulomb stress drop (e.g. Harris 1998; Stein 1999; King and Cocco 2001; Toda et al. 2002, 2012). The primary target of our research is twofold: (1) to investigate the effects of main-shock on the sequence and the strongest aftershock, and

(2) to estimate the post-sequence effects by defining the areas where stress increases and possible triggering may occur, a case which is important for seismic hazard assessment (SHA). The calculation of the static stress changes is based on the Coulomb failure criterion. In more particular, when the Coulomb stress change exceeds a threshold value, slip on fault plane occurs. The aforementioned value is calculated by the following equation:

$$\Delta\sigma_f = \Delta\tau_s + \mu' \times \Delta\sigma_n$$

where $\Delta\sigma_f$ is the Coulomb stress change, $\Delta\tau_s$ is the shear stress change on the failure plane, μ' is the friction coefficient and $\Delta\sigma_n$ is the normal stress change.

Our secondary target is to contribute to the comprehension of the seismotectonic regime of the area, based on the hypocentral relocation, our fault modelling and other published data.

Neotectonic and geodynamic setting

The epicentral area lies on the back-arc basin of the Hellenic Subduction Zone, a tectonic feature that results from the Aegean–Anatolian and African plates convergence. The southwestward tectonic escape of the Aegean–Anatolian plate is also evident by GPS measurements, suggesting a motion of ca. 20 mm/a to the eastern up to 30 mm/a to the western part, relative to Eurasia (e.g. Reilinger et al. 2010; England et al. 2016). The western Turkish coast, from the Biga peninsula to the north down to Rhodes Island to the south, exhibits a N–S dilatation with calculated geodetic strain rates above 50 E09 strain/a throughout the area and up to 140 E09 strain/a locally across the major grabens (Aktug et al. 2009). Within our study area the above authors calculated a strain rate of approx. 60 E09 strain/a which is slightly lower than other estimates for this area (~ 80 E09 strain/a; Jenny et al. 2004; Hollenstein et al. 2008). Although the proposed kinematic elastic block models of Reilinger et al. (2006), Aktug et al. (2009) and Vernant et al. (2014) are quite different, they all suggest a similar block boundary running Gökova Gulf in an E–W direction. According to these models, the estimated slip/motion rates along this boundary are equal to 20.2, 6.6 and 4.0 mm/a for extension, and 8.6, 2.5 and 2.8 mm/a for left-lateral strike-slip, respectively. A 7 mm/a N–S extension is geodetically estimated for this area by Nocquet (2012).

The seismic sequence occurred on the overriding Aegean–Anatolian continental plate, where crust undergoes extension. Due to the complexity of the back-arc area between the subduction zone to the south and the North Anatolian Fault to the north, extension's direction locally varies from NE–SW in the mid-eastern Aegean to a roughly NW–SE axis towards the SE Aegean (e.g. Hatzfeld 1999; Kiratzi and Louvari 2003; Benetatos et al. 2004; Ring et al. 2017). Moreover, within the narrow borders of the study area, extension gradually changes from NW–SE direction east of Kos to roughly N–S direction towards the easternmost part of Gökova Gulf (Hatzfeld 1999; Benetatos et al. 2004; Yolsal-Cevikbilen et al. 2014). Crustal stretching and its consequent tectonic and seismic activity also affect local geomorphology both onshore and offshore. Normal faulting is the most prominent extensional tectonic feature, although significant strike-slip faulting of NE–SW direction is very common at the eastern Aegean (e.g. Zanchi and Angelier 1993; Benetatos et al. 2006; Aktar et al. 2007; Chatzipetros et al. 2013).

Moment tensor solutions (NOA's revised moment tensor catalogue: http://bbnet.gein.noa.gr/HL/seismicity/mts/revised-moment-tensors) confirm the prevailing normal or oblique normal faulting of a broader E–W direction (from ENE–WSW to ESE–WNW), but also reveal quasi-strike-slip faulting of NE–SW direction near Nisyros Island and quasi-normal faulting of approx. N–S direction at western Kos Island (Fig. 2). T-axes have an almost ESE–WNW direction at eastern Kos and Nisyros Islands which turns into NW–SE direction eastwards. At the central part of Gökova Gulf, extension has already changed into N–S direction and further eastwards turns to NNE–SSW direction.

Kos Island and surrounding area

Offshore

Offshore surveys south and west of Kos Island (Pe-Piper et al. 2005; Nomikou and Papanikolaou 2010) revealed several fault systems with different orientations (Fig. 2): (1) ENE–WSW-striking, (2) ESE–WSW-striking, (3) approx. N–S-striking, (4) E–W-striking, and (5) NE–SW-striking fault systems. In fact, there is a gradual change of strike when moving westwards, from ENE–WSW to NE–SW, while ESE–WNW-striking faults occur around the western part of Kos Island also affecting onshore geomorphology. According to Pe-Piper et al. (2005), these faults were developed during three successive tectonic phases that took action since Miocene. The last one, which is still active since Late Pliocene, is responsible for the NE–SW-striking sinistral shear faulting, which also forms extensional Riedel shears.

Onshore

The most prominent morphological feature of Kos Island is Mt Dikaeos, an elongated ENE–WSW-oriented mountain with its highest peak at 843 m a.s.l. Mt Dikaeos mainly consists of Paleozoic (western half) and Mesozoic (eastern half) volcanosedimentary formations (phyllites, pelites and sandstones), which are intruded to the west by a Middle Miocene plutonite (IGME 1998). Narrow parts of the overthrusted (1) Gavrovo tectonic nappe (Upper Jurassic–Middle-Upper Eocene limestones and flysch), and (2) an Upper Tectonic Unit (Lower Jurassic–Cenomanian dolomites, limestones and phyllites-sandstones) can be also found mainly at the northern part of the mountain (IGME 1998). The lowland extends to the northern part of west Kos Island and consists of post-alpidic sediments.

As Nomikou et al. (2018) also propose, both slopes of Mt Dikaeos are bounded by ENE–WSW-striking normal fault zones, forming the ca. 20-km-long tectonic horst. These fault zones consist of parallel, overlapping and down-stepping fault segments, locally affecting the morphological relief.
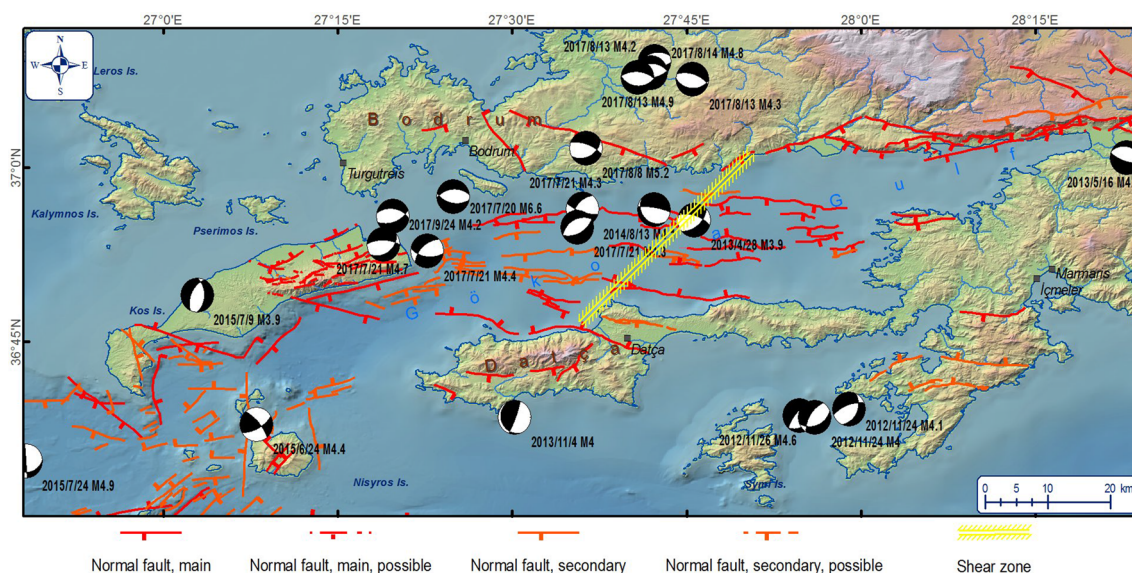
Fig. 2 Tectonic map of the study area combined from Nomikou and Papanikolaou (2010) and Tur et al. (2015) for the offshore neotectonic faults in the SE Aegean and Gökova Gulf, respectively. The shear zone is obtained from Uluğ et al. (2005). The Turkish on land neo-tectonic faults are obtained from Duman et al. (2011) and Emre et al. (2011). Onshore faults of Kos island derive from new field observations and the reassessment of IGME's (1998) 1:50,000 geologic map. Focal mechanisms are from NOA–GI (since 2012)

An approximately 2.2–4.0 km-wide alluvial plain extends north of the mountain range until the northern coastline. The southern slope of Mt Dikaeos is locally steeper than the northern one implying a faster uplift along the southern side of the island. Both slopes have developed parallel drainage networks superimposed on the alpidic and post-alpidic formations (Fig. 3). The northern networks locally show diversions or asymmetrical development which many times are due to tectonic causes. The southern ones, as expected, are much shorter and locally sparser without any change in direction.

From a morphotectonic point of view, the northern side is cut by a series of parallel, down-stepping normal faults controlling the mountain-front. Swath profiling across the northern slope (Fig. 3) shows narrow tectonic terraces and knick-points between successive overlapping faults that run parallel the foothills. Normal fault growth and interaction investigations using the relationship between fault length and displacement (e.g. Cowie and Scholz 1992; Cartwright et al. 1995; Gupta and Scholz 2000) have shown that individual fault growth produces a roughly elliptical cumulative displacement along strike. When another adjacent individual fault segment starts to interact, displacement's elliptical shape of one or both segments becomes disturbed, until the two segments are breached. Along the northern slope of Dikaeos Mountain, longitudinal swath profiles depict two cumulative displacement elliptical shapes, suggesting the existence of two fault segments, 'A' and 'B' (Fig. 3). In fact, it seems that segment 'B' tends to interact with the western segment 'B'. Similar tectonic pattern is also met at the

southern slope of Dikaeos Mountain. Swath profiles perpendicular to the slope suggest the occurrence of a SSE-dipping normal fault array. Considering the occurrence of a parallel to the coast, offshore fault (Nomikou and Papanikolaou 2010), and comparing the northern and southern side slope gradients, it is also implied that a faster uplift occurs along the southern side of the island.

The Gökova Gulf

Gökova Gulf, an E–W-trending graben (Yilmaz et al. 2000) of late Pliocene–early Pleistocene age (Tur et al. 2015), is located between Bodrum and Datça peninsulas and extends for ca. 100 km on an E–W axis with a N–S opening of ca. 25 km. Onshore normal faults are evident along both northern and southern margins of Gökova Gulf (Fig. 2; e.g. Yilmaz et al. 2000; Gürer and Yilmaz 2002; Altunel et al. 2003; Duman et al. 2011). The northern margin (Bodrum peninsula) is characterized by a steep linear mountain front cut by E–W- and NW–SE-striking faults. The southern margin (Datça peninsula) demonstrates a much more subdued relief and a fewer number of faults. Based on focal mechanism calculations, Yolsal-Cevikbilen et al. (2014) recognised only extensional tectonics with a small amount of strike-slip component and T-axis direction ranging between N–S and NW–SE.

Offshore surveys in the Gökova Gulf have revealed a tectonically affected seafloor (Kurt et al. 1999; Uluğ et al. 2005; İşcan et al. 2013; Tur et al. 2015; Ocakoglu et al. 2018). Tur et al. (2015) calculated an average subsidence rate of the gulf
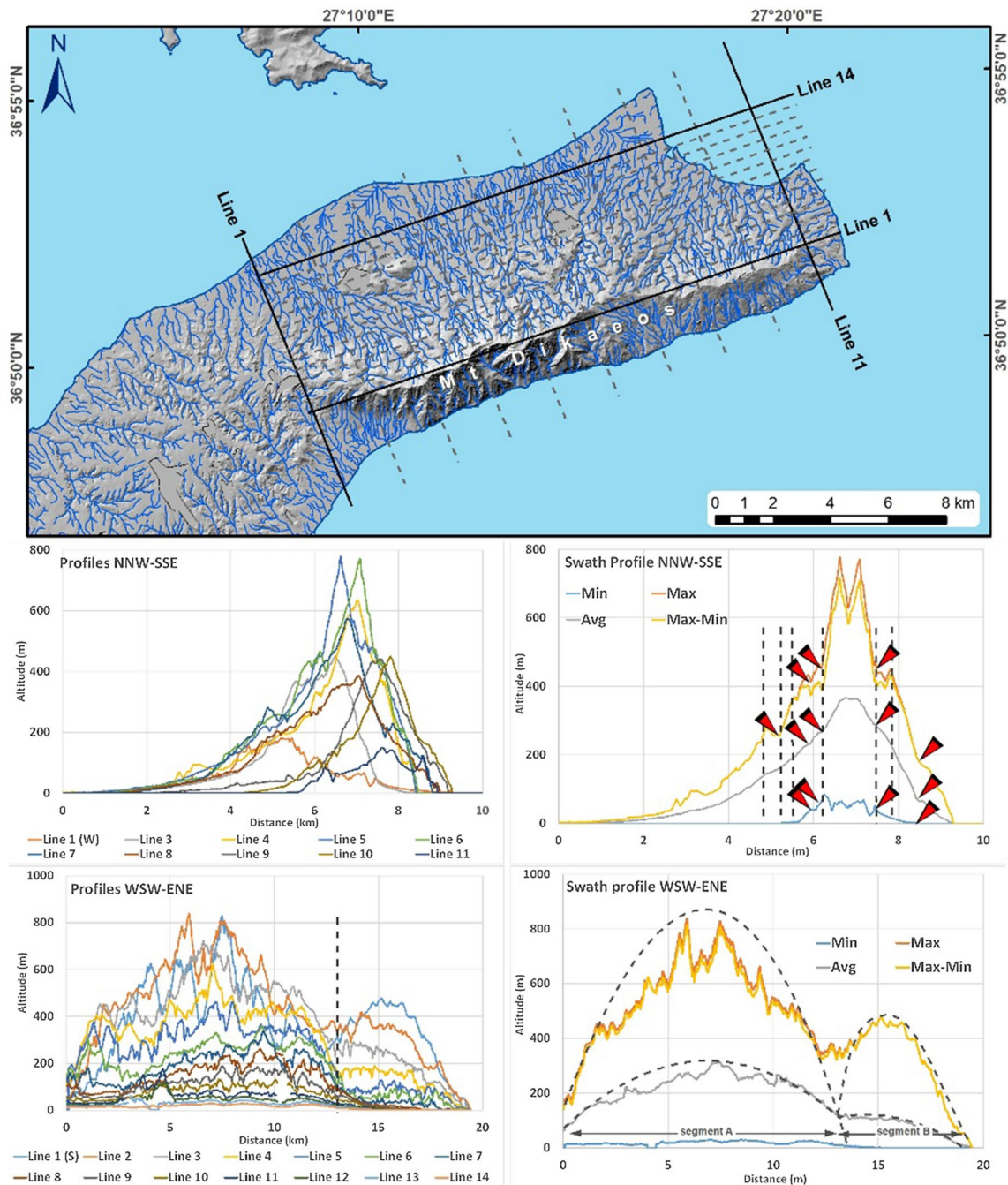
Fig. 3 (*Top*) DEM (5 m resolution from the Hellenic Cadastre) of eastern Kos Island. Drainage network is produced automatically with manual corrections. Dashed lines correspond to the topographic swath profiles below. (*Bottom*) Topographic swath profiles longitudinal (WSW–ENE) and transversal (NNW–SSE) to Dikaeos Mountain range. The sets on the right show the minimum, average, maximum and the maximum minus the minimum values of the swath profiles. Red arrowheads and dashed black lines in the NNW–SSE swath profile inset mark faults location and tectonic terraces width, respectively. More explanations in the text

at ~ 0.8 mm/a and a differential counter-clockwise rotation of 1.5° during the last 500 ka for the eastern part of the gulf and 3° during the last 1.5 Ma for the western one. They also conclude that the western part of the Gökova Graben is older and subsides faster than the eastern one. Based on seismic-reflection profiles and multibeam bathymetry, the authors

recognized three distinct fault orientations in the area, both offshore and inland, with prominent morphological expression: (1) NW–SE-striking faults that delimit margins of the submarine rhomboidal basins, (2) broadly E–W-striking low-angle normal faults that bound the present-day shoreline and the morphological structures in the western part of the gulf,

and (3) the ENE–WSW-striking normal faults that occur along the northern shoreline of the gulf. İşcan et al. (2013) support that the seafloor morphological structures are the result of compressional deformation due to the presence of shear faulting. According to Kurt et al. (1999), the most prominent tectonic structure in the gulf is the offshore, N-dipping, (low angle) listric 'Datça' blind normal fault, which delineates the southern margin. The authors, and later Uluğ et al. (2005), suggested that the 'Datça' fault is responsible for the opening of the gulf since the Latest Miocene-Pliocene, but its activity has been decelerated, giving space for WNW–ESE- and major E–W-striking faults to develop on the hanging-wall. Moreover, Tur et al. (2015) concluded that the 'Datça' fault has gone to inactivity since late Pliocene. On the contrary, based on seismological data, Rontogianni et al. (2011) argue about the activity deceleration of the fault suggesting that there is a probable connection between a young NE–SW-striking sinistral transfer fault, the Gökova Transfer Fault (GTF), and the 'Fault of Kos'. The existence of the GTF in the middle of the gulf was initially proposed by Uluğ et al. (2005) and was later supported by other researchers (İşcan et al. 2013; Ocakoglu et al. 2018). This tectonic feature is considered similar to the parallel Fethiye–Bordur sinistral shear zone (e.g. Taymaz and Price 1992; ten Veen 2004; Ocakoğlu 2012; Hall et al. 2014; Elitez et al. 2016), which lies just some tenths of kilometres further to the east. On the other hand, Tur et al. (2015) suggest that this NE–SW-trending structure in the gulf is misinterpreted and it represents the continuation of a prominent arcuate normal fault. A twofold interpretation is given by Ocakoglu et al. (2018) for the NE–SW-trending morphological features, besides the existence of the GTF: (1) the faults east of Kos Island are the continuation of the E–W-striking normal faults at the inner part of the gulf that keep their kinematic character, and (2) the faults moving towards the middle of the gulf suddenly become sinistral strike-slip that cut and displace the E–W-striking normal faults, implying being younger structures. It is not explained, however, the reason of the suddenly change in kinematics of these two fault groups.

It is obvious from the above that there are many tectonic interpretations for the Gökova Gulf. The diversity of regional focal mechanisms (Fig. 2) supports the occurrence of a variety of faults in both terms of kinematics (ranging between almost left-lateral strike-slip and normal dip-slip motion) and geometry (various fault directions, from E–W to NE–SW, or even N–S at the eastern part of the study area).

The 2017 seismic sequence

Seismological data

The mainshock occurred on July 20, 2017, at 22:31:11.0 (UTC) and was preceded (21 min earlier) by a M_L 2.9

foreshock near to the mainshock's epicentre. Numerous aftershocks followed, the strongest of which occurred on August 8, with a magnitude of M_W 5.3.

The source parameters of the mainshock, given by IG–NOA's moment tensor solution, are shown in Table 1. The solution suggests quasi-E–W-striking, moderate dipping, normal faulting, and it is compatible with other proposed focal mechanisms (KOERI, USGS, GFZ, GCMT, INGV, UoA and AUTh). Nevertheless, the moment tensor alone is not enough to resolve which nodal plane is responsible for the mainshock.

We relocated the seismic sequence of Kos using combined P- and S-wave phase data from the HUSN (Hellenic Unified Seismograph Network) and the KOERI (Kandilli Observatory and Earthquake Research Institute) networks. During the period of 5/7/2017 to 31/10/2017 more than 11,000 events were recorded in the broader region of the main shock. Our initial dataset consisted of more than 110,000 P and 47,000 S phases recorded by the stations of HUSN and KOERI networks.

The nonlinear location algorithm NonLinLoc (Lomax et al. 2000) was used for the event location procedure. The Posterior Density Function (PDF) of the solution is calculated using the equal-differential-time (EDT) likelihood function (Font et al. 2004) with which the travel-time difference between observed and synthetic travel times is calculated for pairs of stations, contrary to typical least squares methodologies. The advantage of this method is that the solution is independent of the origin time, and thus the problem is reduced to a 3-D search over space. Furthermore, this methodology makes it possible to identify mispicked data and exclude them from the final location solution. The search for the optimal location is performed throughout the whole space using the Oct-tree importance sampling algorithm (Lomax and Curtis 2001) which uses recursive subdivisions of a gridded space. This eliminates the issue of location error due to local minima in the PDF.

The relocation procedure was based on the 1-D velocity model proposed by Panagiotopoulos et al. (1985). In our final dataset (Fig. 2) we selected all events with more than 15 phases, located with azimuthal gap < 180°, location RMS < 1 s and horizontal and vertical errors < 2.5 km.

The hypocentral relocation reveals two main clusters (Fig. 4), an eastern and a western one (clusters 'A' and 'B', respectively), which is in accordance with patterns suggested by Karasözen et al. (2018), Ganas et al. (2019) and Konca et al. (2019). The eastern cluster can be divided into three sub-clusters. Sub-cluster 'A1' is allocated along an E–W-trending axis for a distance of almost 10 km long and shows a N-dipping trend (profile C–C′ in Fig. 5). Sub-cluster 'A2' is tangential to 'A1', but allocated along a NNW–SSE-trending axis for a shorter distance (ca. 7.5 km) and shows a NE-dipping trend (profiles C–C′

and D–D′ in Fig. 5). Sub-cluster 'A3' is located south of the previous two; it is sparser and it does not demonstrate any particular trend. Sub-cluster 'A3' is less concentrated and clearly separated from 'A1' and 'A2' (profile C–C′ in Fig. 5).

Eastern cluster 'B' extends for almost 16 km (map view in Fig. 4 and profile B–B′ in Fig. 5) in a roughly E–W direction and shows a clear N-dipping trend (profile A–A′ in Fig. 5). It represents the rupture length of the mainshock.

The vertical distribution of the sequence suggests that the maximum number of events occurred at the depths of 8–9 km (28.7% of total aftershocks). Besides sub-cluster 'A2', all other clusters reach maximum depths of approximately 15 km (Fig.6). Mainshock's and strongest aftershock's relocated hypocentral depths are calculated to 9.3 and 8.0 km, respectively.

Spatio-temporal evolution of the aftershock sequence (Fig. 4) shows that 1 day after the event, only sub-cluster 'A3' started to develop, while cluster 'B', i.e. the epicentral area, is much poorer in events. This contrast goes on for almost one week, after of which sub-cluster 'A1' started to develop, while cluster 'B' became richer. Approximately one month after the mainshock all clusters and sub-clusters had been adequately developed. The spatio-temporal evolution indicates different behaviour in the clusters development which is probably due to stress loading and successive reactivation of different tectonic structures.

GPS-based geodetic data

The use of satellite geodesy is a reliable way of estimating the upper crust deformation, related to the fault zones activity or the occurrence of a seismic event. In particular, the study area is monitored by a dense GPS/GNSS network, including 10 continuous-permanent stations (7 in Turkish and 3 in Greek area) and 5 campaign-surveyed stations (Fig. 7; Tiryakioğlu et al. 2018).

The recorded coseismic displacements close to the epicentral area are significant, presenting values ranging between 19 and 153 mm for the North component, and between 9.2 and 39.4 mm for the East one (Tiryakioğlu et al. 2018). The interpretation of these measurements suggests that the main event is developed in a N–S-striking motion, being in an agreement with the N–S extensional regime of the area; thus, they can be correlated to an E–W-striking, normal seismic fault (Tiryakioğlu et al. 2018). In addition, the effect of coseismic displacement in the vertical component was limited, while stations located 50 km or more from the mainshock epicenter recorded minor values (Tiryakioğlu et al. 2018).

Table 1 Moment tensor solution for the July 20, 2017 mainshock by IG–NOA

| Event | Centroid lat (°N) | Centroid long (°E) | Centroid depth (km) | M_W | M_0 (Nm) | Nodal plane 1 | | | Nodal plane 2 | | | P-axis | | T-axis | |
						Strike (°)	Dip (°)	Rake (°)	Strike (°)	Dip (°)	Rake (°)	Azimuth (°)	Plunge (°)	Azimuth (°)	Plunge (°)
July 20, 2017 mainshock	36.9585	27.415	6	6.6	8.928 E18	265	43	−102	102	48	−79	76	81	184	3

Fig. 4 (*Top*) Hypocentral relocation of the 2017 seismic sequence (after Sboras et al. 2018). Light blue and yellow stars mark the mainshock and the second strongest shock. Focal mechanism of the main-shock is by IG–NOA. Three sub-clusters, A_1, A_2 and A_3, can be distinguished east of the Karaada Is., and a main cluster B around the epicentral area, west of the Karaada Is. (dashed red outlined ellipses). Path lines correspond to the vertical profiles of Fig. 5. (*Bottom*) Spatio-temporal aftershock evolution one day (24 h), two days (2 d), one week (1 w), two weeks (2 w), one month (1 m) and until 30/10/2017 (light blue star = mainshock)
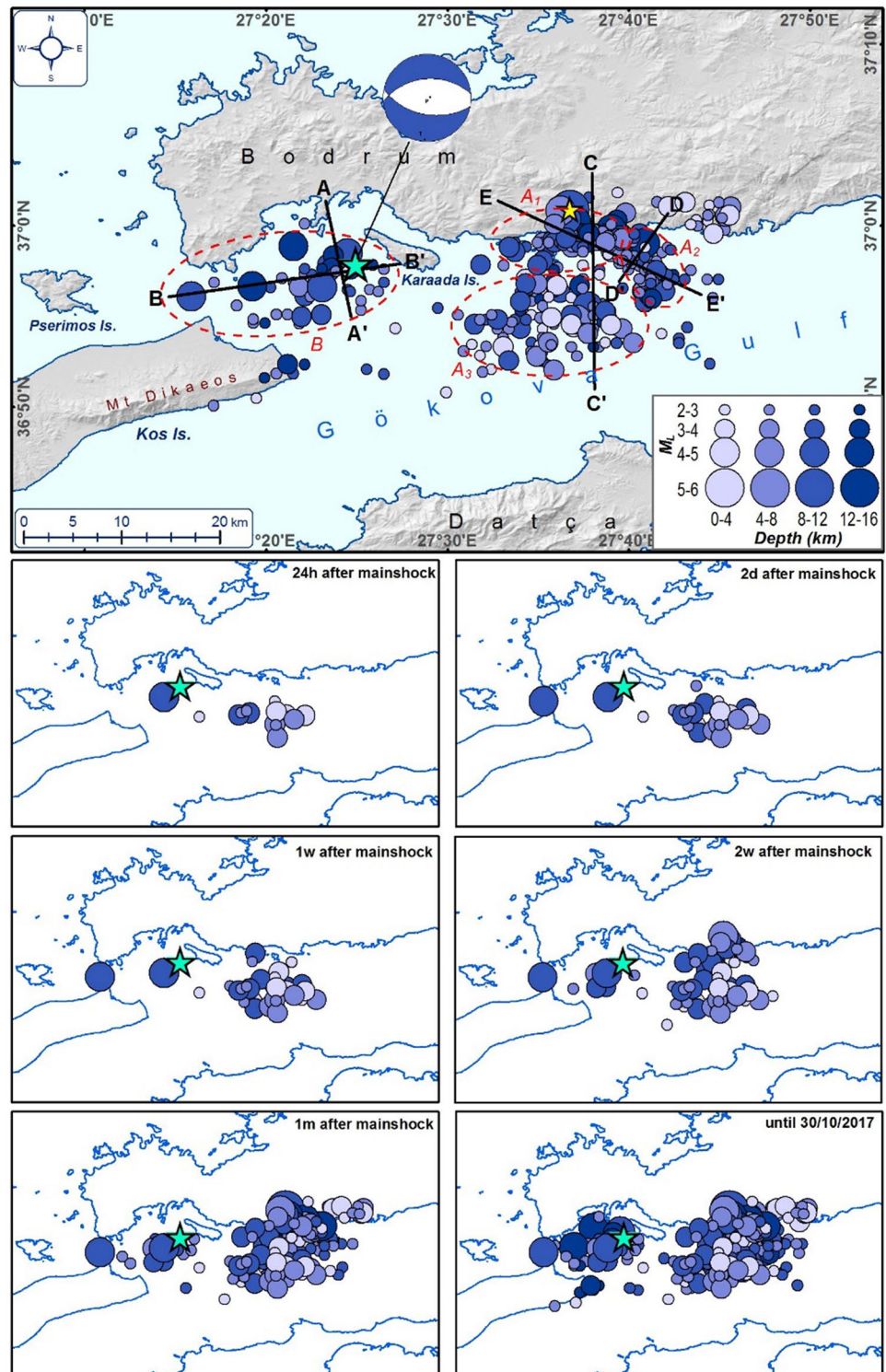

Ground deformation effects

Primary ground deformation effects were not observed, on either Kos Island or the Turkish coast. However, several secondary effects were recorded on both areas.

On Kos Island, the secondary ground deformation effects were constrained at the eastern part of the island (Sboras et al. 2018; Papathanassiou et al. 2019). These effects included liquefaction-related phenomena (sand volcanos and lateral spreading) and secondary ground fissures. Landslides

Fig. 5 Vertical hypocentral distribution along the paths shown in Fig. 4. Blue star corresponds to the mainshock
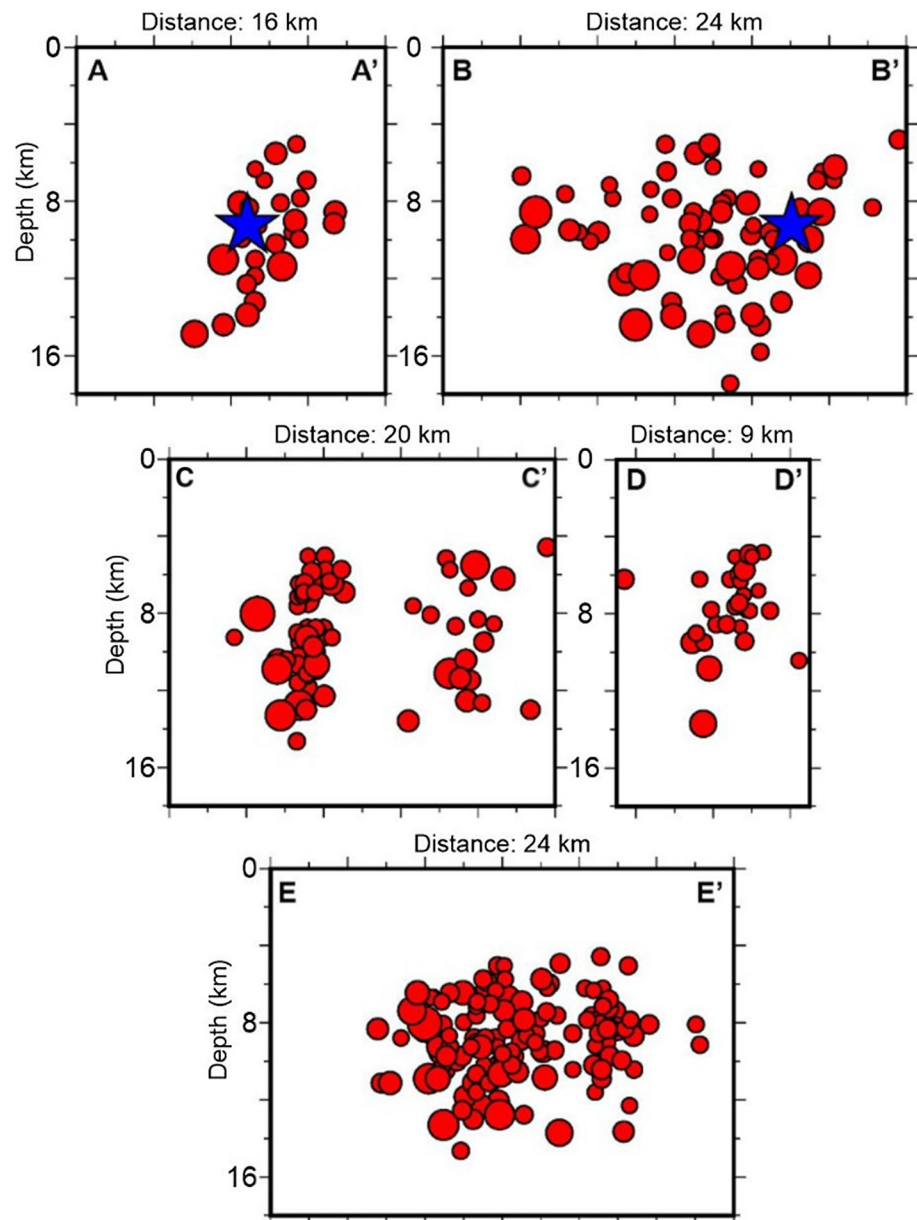
and rockfalls were limited and no primary ground ruptures were observed.

Along the Turkish coast, there is information only for a tsunami occurrence. According to field surveys (Yalçiner et al. 2017; Dogan et al. 2019), a tsunami hit the southern coast of Bodrum peninsula causing damage. The maximum impact was recorded at Gumbet Bay (west of Bodrum town). On Kos Island, 1.5 m-high tsunami wave was measured in the port (Dogan et al. 2019).

Source modelling

The preferred slip model of the mainshock proposed by Kiratzi and Koskosidi (2018) suggests, but not exclusively,

a S-dipping (~50° dip) fault plane with two shallow slip patches, an average slip of 50 cm, plane dimensions of ~30 km (length) by 15 km (down-dip width) and a moment of $M_0 = 1.214$ E19 Nm (Table 2). The selection of the S-dipping fault plane was based on morphology and the research of Ocakoğlu et al. (2018). This model opposes the N-dipping trend of the aftershocks' spatial distribution. The less preferred model of the authors is a N-dipping fault plane (Table 2) on which the peak slip values are calculated towards its western part.

Ganas et al. (2019) modelled a NNE-dipping, blind seismic source, with 14 km length and 12.5 km width and upper depth at 2.5 km. Their model is mainly based on GNSS and InSAR inversion. The seismic source is located between the

Fig. 6 Depth distribution of the 2017 Kos–Bodrum aftershocks (histogram). The maximum number of events is located at a depth of 8–9 km, where the mainshock's and strongest aftershock's hypocentral depths are relocated (9.3 and 8.0 km, respectively)
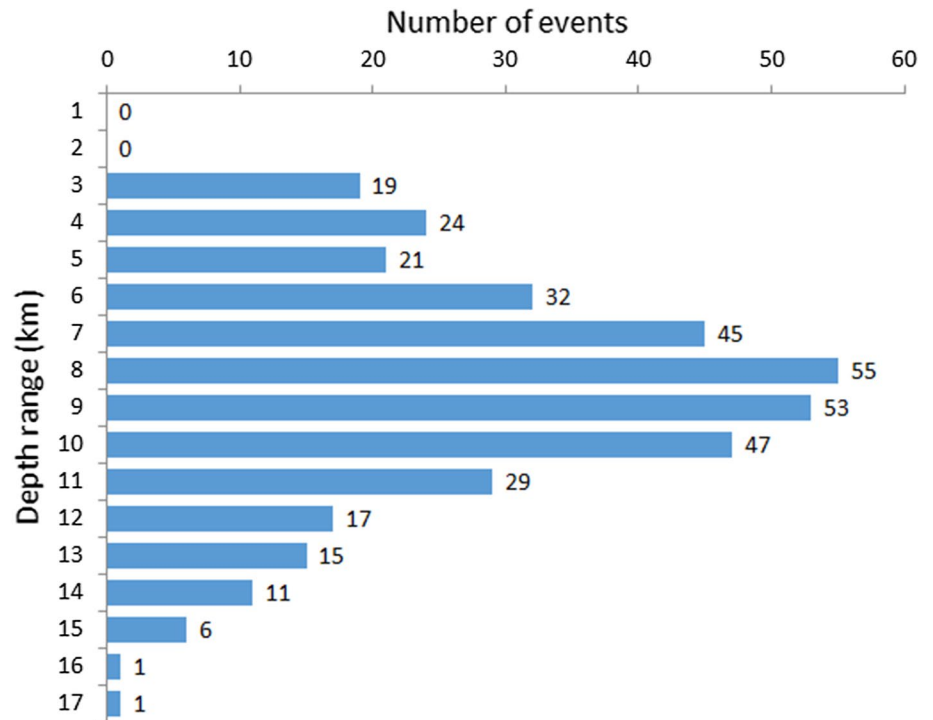

Fig. 7 Coseismic displacements, recorded by GPS/GNSS stations (modified from Tiryakioğlu et al. 2018)

two aftershock clusters 'A' and 'B' (Fig. 4, top) as the result of stress increase (off-fault aftershock clusters). However, the uneven spatio-temporal evolution of the two clusters (Fig. 4, bottom) makes this scenario less credible.

The source model of Saltogianni et al. (2017) suggests a S-dipping fault plane based on GPS data inversion and the moment tensor of the mainshock. This model comes in contrast with the N-dipping trend of the relocated aftershock sequence.

For the purposes of tsunami modelling, Dimova and Raykova (2018) proposed three (3) candidate tsunamogenic fault models, based on focal mechanisms (GFZ and

Table 2 Proposed fault models for the July 20, 2017 mainshock

No	Strike	Dip	Rake	Length (km)	Width (km)	Upper depth (km)	Average slip (m)	References
1	098.0°	~50.0	−98.0	30.0	15.0	0	0.5–0.6	Kiratzi and Koskosidi (2018)[1]
2	284.0°	32.0°	−71.0	30.0	15.0	0	0.5–0.6	Kiratzi and Koskosidi (2018)[2]
3	095.0°	56.0°	−98.0	25.0	14.5	0	–	Saltogianni et al. (2017)
4	283.0°	37.0°	−75.0	14.0	12.5	2.5	2.03	Ganas et al. (2019)
5	274.9°	36.5°	−79.5	16.8	13.3	1.2	1.46	Karasözen et al. (2018)[3]
6	274.9°	36.5°	−79.5°	30.0	16.8	0	1.8	Karasözen et al. (2018)[4]
7	285.0°	39.0°	−73.0°	25.0	15.0	7.0	0.4	Heidarzadeh et al. (2017)[5]
8	84.0°	53.0°	−103°	25.0	15.0	7.0	0.4	Heidarzadeh et al. (2017)[6]
9	265.0°	43.0°	−102.0°	26.0	15.0	4.0	0.68	Sboras et al. (2018)
10	270.0°	56.0°	−94.0°	33.0	17.0	1.0	2.5	Dimova and Raykova (2018)

[1]Best S-dipping model (preferred)

[2]Best N-dipping model (alternative)

[3]Uniform slip

[4]Variable slip

[5]N-dipping plane

[6]S-dipping plane

GCMT). The most favourable scenario uses a N-dipping fault (Table 2) after comparing the results with recorded sea level elevations from the Bodrum station.

Our model, initially published in 2018 (Sboras et al.) and slightly modified in this paper, is mostly based on seismological data. The source dimensions are estimated at 26 km length and 15 km width, using the scalar relationships of Wells and Coppersmith (1994). Strike, dip and rake are obtained from NOA's focal mechanism (Table 1). The vertical position of the fault plane is based on the lack of any primary ground ruptures and on the vertical distribution of the western cluster 'B', which shows that it was restricted approximately between the depths of 4 and 14 km. The relocated hypocentre of the mainshock also constrained the N–S horizontal positioning of the source. The horizontal positioning depends on (1) the horizontal relocated aftershock distribution, and (2) the ground deformation observed on the southeastern edge of Kos Island as revealed by InSAR images (Ganas et al. 2019). The NNW-dipping fault segment along the northern front of Mt Dikaeos (Kos Island) is probably the surficial expression of the geological fault, part of which is the seismic source of the 2017 mainshock. An average slip of 0.68 m is calculated from M_0 and the source dimensions after applying the formula of Aki (1966): $M_0 = \mu \cdot u \cdot L \cdot W$ (μ is shear modulus, u is average slip, L is length and W is width). Thus, we suggest a N-dipping normal fault plane for the mainshock. The model was also tested by Sboras et al. (2018) after comparing the theoretic surface deformation, based on Okada's (1992) formulae, with the deformation calculated in InSAR images (Ganas et al. 2019). Moreover,

a N-dipping fault provides better results in the tsunami model scenarios of Dimova and Raykova (2018).

The two sub-clusters A_1 and A_2 (Fig. 4) obviously correspond to two different active tectonic structures within the Gökova Gulf. Sub-cluster A_1 also includes the second strongest shock (M_W 5.3) which occurred on August 8 and whose hypocentral depth is calculated at ca. 8 km. Although GFZ's centroid epicentre is located few kilometres south from the relocated epicentre, the proposed nodal planes reveal E–W-striking, almost pure normal faulting (Fig. 8). Given that sub-cluster A_1 dips to the North (profile C–C', Fig. 4 and Fig. 5), our preferred model for this event is a N-dipping normal fault (Table 3) which also matches the offshore tectonic pattern of the Gökova Gulf (Tur et al. 2015; Fig. 2). Sub-cluster A_2 delineates a NW–SE-striking fault dipping to the NE; however, there is neither a significant event nor a focal mechanism in order to model this tectonic structure.

Coulomb static stress changes

Methodological approach

We used the Coulomb failure criterion (see Introduction) for two different cases:

Case A Our first target is to examine how the mainshock affected the aftershock sequence and especially the strongest aftershock, also validating our mainshock's fault model. Thus, we used fault model F1 as the only slipping fault
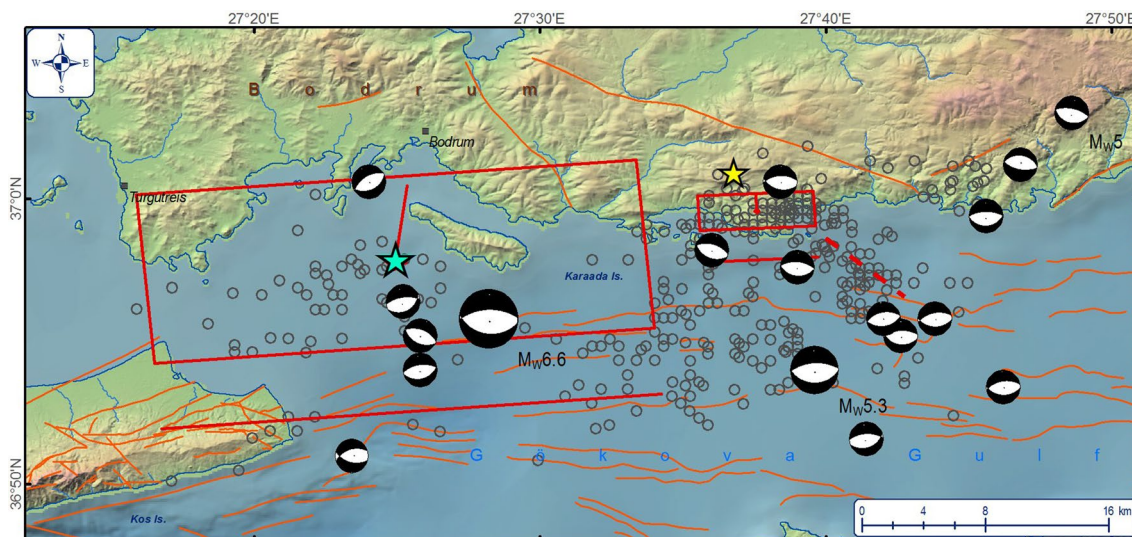
Fig. 8 Map showing the two modelled seismic faults (seismic sources) of the two strongest shocks during the 2017 Kos–Bodrum sequence. The rectangular represents the vertical projection of the fault plane; parallel line represents the section of the upward fault plane prolongation and the map plane; line in the centre of the fault plane shows the slip direction. The dashed, toothed red line corresponds to a NE-dipping fault detected from the relocated hypocentral distribution (cluster A₂). Focal mechanisms are obtained from GFZ Potsdam (main and second stronger shocks are proportionally over-sized). The relocated epicentres are shown in grey circles. Light blue and yellow star correspond to the epicentres of the main and second stronger shocks of the sequence. Orange lines stand for the geological faults recognised in the area

Table 3 Seismic source main parameters of the two strongest shocks of the 2017 Kos earthquake sequence

Source	Strike (°)	Dip (°)	Rake (°)	Length (km)	Width (km)	Min depth (km)	Max depth (km)	Average slip (m)	M_0 (Nm)
F1 (mainshock)	265	43	− 102	26.0	15.0	4.0	14.2	0.68	9.0E+18
F2	267	63	− 91	6.0	5.0	4.0	8.5	0.17	1.7E+17

(source fault) and fault model F2 as a receiver fault (Fig. 8 and Table 3). Our primary concern was to calculate the Coulomb stress changes near the strongest aftershock's hypocentral depth, i.e. 8 km. Nevertheless, further calculations are needed in order to examine the whole sequence spatial distribution.

Case B Based on our knowledge of the seismotectonic regime of the area (Fig. 2), both on land and offshore, we also focus on estimating possible triggering (or delay) effects caused by the combined reactivation of both fault models F1 and F2. Based on the fact that (1) stress changes depend on the geometry (strike and dip) and kinematics (rake) of the receiver faults, and (2) the dominating fault system in the area is the E–W-striking normal faults, we preferred to calculate the static stress changes for the aforementioned fault system as receiver faults (assuming a moderate dip angle of 45°) at three different depths of 8, 10 and 12 km. It must be mentioned that dip direction does not significantly change

the stress change pattern; thus, we expect similar patterns for either north- or south-dipping faults.

Results

Case A Our in-sequence investigation shows that fault model F2 lies entirely within the crustal volume where stress rises (Fig. 9). The on-fault calculations (Fig. 9) show that the minimum values (ca. 1 bar) occur on the top eastern corner of the fault plane, whereas the maximum ones (ca. 3 bar) occur on the opposite corner. The area bilaterally of F1's fault plane is dominated by stress drop, while from all tips (upper, lower, east and west) and beyond stress increases. Aftershock spatial distribution can be separated into two groups: the aftershocks that closely surround F1's fault plane (matching cluster B of in our previous discussion, see Fig. 4) and the aftershocks that mostly comprise cluster A. The former is quite sparse and located within the stress-drop crustal
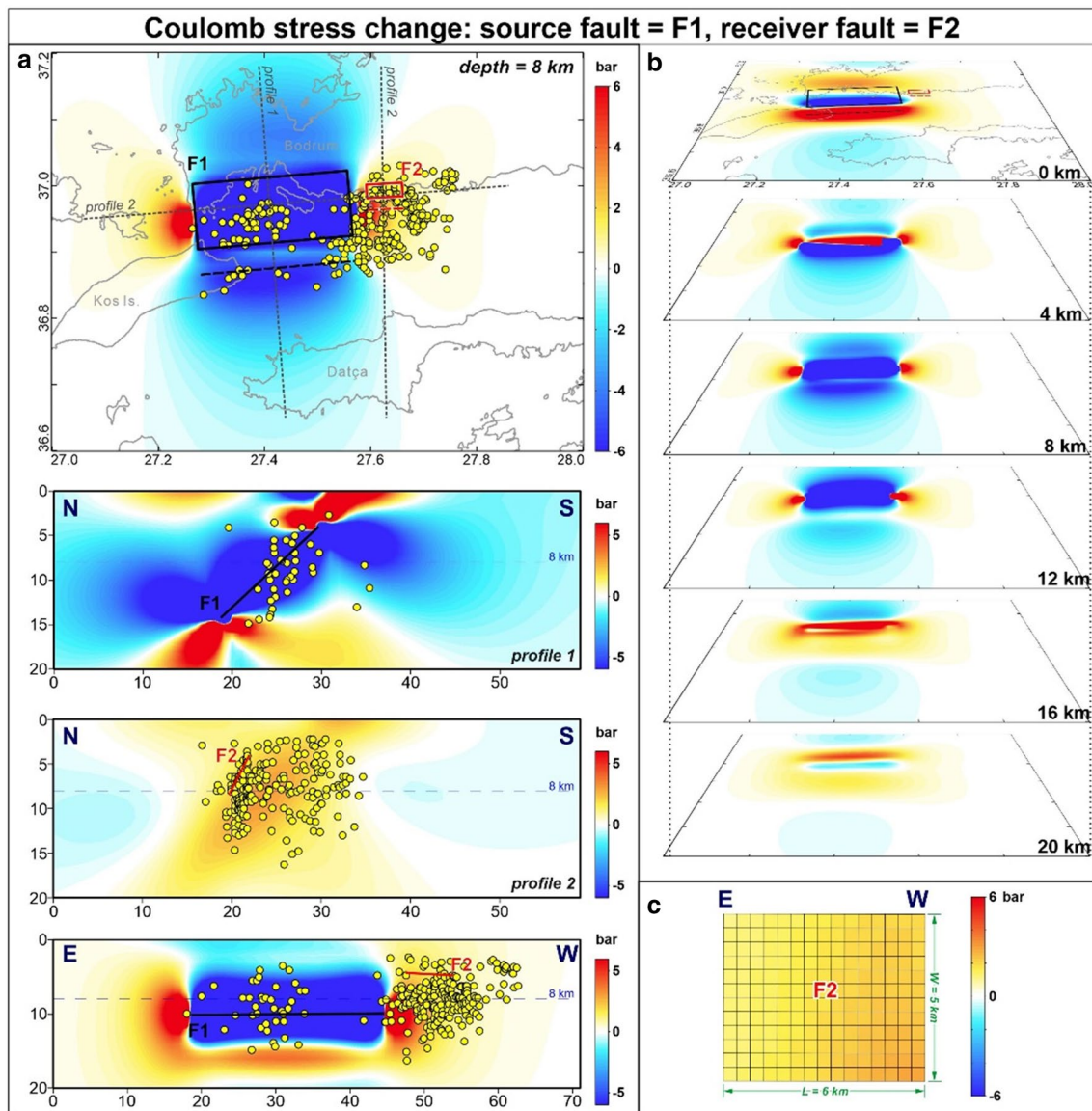
Fig. 9 Coulomb static stress changes calculated for the 2017 Kos–Bodrum earthquake sequence using fault model F1 (mainshock) as source fault and fault model F2 (strongest aftershock) as receiver fault. **a** Stress changes on a map view (top) for the depth of 8 km (close to the hypocentral depth of the strongest aftershock), and on vertical cross sections (profiles 1, 2 and 3). The relocated hypocentres are also plotted. **b** Sequential stress change calculations (in 3D map view from the south) from surface to the depth of 20 km with 4 km intervals. **c** Stress change on fault's F2 plane after dividing the surface in 180 tiles (15 along strike and 12 along width). View from hanging-wall

volume. On the contrary, the rich, denser cluster B, with all its sub-clusters, is almost totally located within the stress-rise crustal volume.

Case B Our post-sequence investigation for faults in Group A shows that E–W-striking faults within the Gökova Gulf and immediately east of fault F1 are loaded with stress (Fig. 10). Stress rise is extended not much to the east, leaving unaffected similar faults that lie in the middle and eastern part of the gulf. Faults of Group A that are located south of fault F1 (or north, if any exist) are relieved from stresses. Underneath fault F1, stress load occurs only at greater depths, i.e. 14 km (Fig. 10).

Discussion

The seismic sequence took place near to the border of the back-arc N–S extensional regime, which controls the western coast of Turkey (e.g. Hancock and Barka 1987; Cohen
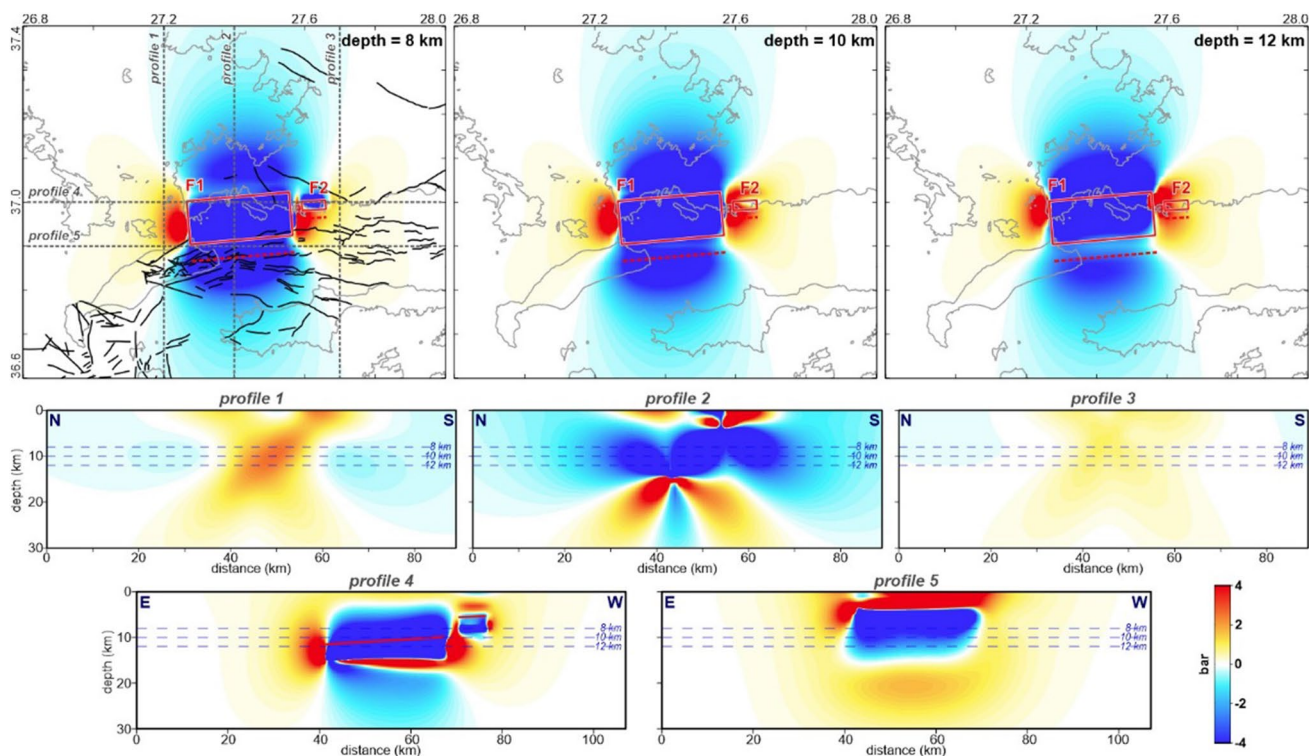
Fig. 10 Coulomb static stress changes calculated after the activation of seismic sources F1 and F2 for receiver faults of E–W strike, moderate (45°) dip and pure normal kinematics. Top row: Horizontal sections at depths of 8, 10 and 12 km; black lines represent all faults in the study area. Middle row: N–S profiles. Bottom row: E–W profiles

et al. 1995; Gürer et al. 2009), the large NE–SW-striking Burdur–Fethiye shear zone further to the southeast (e.g. Hall et al. 2014; Elitez et al. 2016), which is part of the Isparta Angle, and the NE–SW-striking shear zones that seem to dominate the southeastern Aegean Sea (just west of Kos and Nysiros islands; e.g. Mascle and Martin 1990; Pe-Piper et al. 2005; Tsampouraki-Kraounaki and Sakellariou 2017). Morphotectonic features and focal mechanisms in the epicentral area of both diachronic seismicity and the latest 2017 sequence suggest that the roughly N–S extension prevails, besides the occurrence of the NE–SW-striking shear zones immediately west of Kos Island (Sakellariou and Tsampouraki-Kraounaki 2019 and references therein). Thus, from a kinematics point of view, the Island of Kos probably marks a stress and fault direction change point toward the west, as its morphological pattern implies as well. Our tectonic interpretation in the 2017 epicentral area shows no significant differentiation with the diachronic focal mechanisms and the fault pattern in the Gökova Gulf (Fig. 2). Could the 2017 seismic fault be part of the separating boundary between two geodetically rigid blocks? Its N-dipping direction and its continuation on land Kos Island, north of Mt Dikaeos, probably rule out such a consideration. Spatial epicentral distribution since 2008 (Fig. 1) shows a quite long (several tens of kilometres), ENE–WSW alignment at the middle of the

gulf, matching the on land geologically determined tectonic pattern of the area. Perhaps this structure plays an important role in the gulf and local tectonics; its nature, however, is unknown. In contrast with the above regime, a group of scientists supports the occurrence of a left-lateral shear zone that 'splits' the gulf diagonally, from NE to SW, based on marine surveys. A question still remains: is the Gökova Gulf affected by the Hellenic Arc curvature and how?

The 2017 earthquake sequence shows no evidence of a NE–SW-striking shear zone, although the location of horizontal distribution was limited just east of the proposed zone. It is unfounded to say whether the spatial distribution was limited due to the occurrence of the shear zone or the lack of any stress load. Moreover, the relocated aftershock distribution does not depict any NE–SW-striking tectonic structures and all moment tensors demonstrate quasi-pure normal faulting mostly on ca. E–W-striking faults.

The spatio-temporal evolution of the 2017 sequence (Fig. 4) showed an asymmetrical seismic evolution, with cluster 'A' being significantly enriched immediately after the mainshock on July 20. It took more than one week for cluster 'B' to practically start developing. Until the end of October, both clusters had been developed, but with an explicit difference in the number of events. It is noteworthy that seismicity around the main fault F1 is mostly constrained near, and

practically surrounds, the fault plane. A possible explanation for this effect is that, after the July 20 mainshock, the rupture of fault F1 immediately loaded the eastern area with stresses, while the fault itself was considerably relieved, preventing the occurrence of further aftershocks along the fault plane until some stresses slowly started to develop producing the late seismicity of cluster 'B'. The stress load at the eastern tip of the main fault facilitated the neighbouring tectonic structures to develop notable seismicity. It is noteworthy that west of the mainshock-inducing fault F1 (offshore, north of Kos Island) seismicity entirely lacks, possibly also implying either the absence of any tectonically active structures, or the occurrence of a different local geodynamic/seismotectonic regime that does not allow interactions in between. However, the mapped onshore faults of Kos Island show no further aftershock activity, probably due to the stress drop that covers this area.

Highly notable is the NW–SE-striking, NE-dipping tectonic structure detected only by the relocated aftershock spatial distribution (corresponding to sub-cluster A_2; Fig. 4). Other faults with similar orientation have been detected in the broader area, however without representing the dominating tectonic structures. This particular fault is located immediately east of the E–W-striking fault F2, possibly preventing the latter to extend further to the east.

Field observations and morphotectonic evidences on eastern Kos Island imply that the N-dipping faults are the upward prolongation of the 2017 earthquake rupture surface, although rupture never reached the surface. If we consider that older earthquakes might have ruptured the surface, the total fault dimensions may be greater than the 2017 rupture, which implies a greater magnitude potential. Estimations from historic events suggest quite high magnitudes up to M 7.0 near Kos Island and M 6.8 at the far eastern margin of Gökova Gulf (Papazachos and Papazachou 2003; Fig. 1); these old, prior to the twentieth century, earthquakes, however, involve significant errors in both magnitude and location estimation. The rich seismic history near Kos Island could be related to the on land faults of the island, even though both the N- or S-dipping faults can be responsible for these events. The central part of Gökova Gulf does not demonstrate any significant historic events; only two moderate events were instrumentally recorded in 2004 at the order of M_L 5.0. On the seismicity map of the last ca. 10 years (and before the 2017 sequence, Fig. 1), an ENE–WSW-trending elongated seismic cluster is formed, parallel to the fault F1's strike, suggesting that this orientation of faulting prevails in this particular part of the study area.

The geodetically constrained fault geometry and the off-fault aftershock process suggested by Ganas et al. (2019) matches neither the seismological data (focal mechanism, spatial distribution) nor it can explain why the western and eastern clusters developed so differently from each other.

Our seismologically, and less geologically, constrained model better fits the aforementioned geometric criteria and supports the on-fault aftershock evolution.

Conclusions

The July 20, 2017 mainshock ruptured a N-dipping fault plane near the northern margin of Gökova Gulf, at the eastern part of Kos Island, in contrast to the prevailing S-dipping tectonic structures that control the coastline. The mainshock triggered minor adjacent tectonic structures east of the epicentral area which can be clearly detected from the spatial hypocentral distribution. The on land N-dipping faults mapped on eastern Kos Island probably belong to the same tectonic structure which produced the 2017 earthquake, even though the latter never ruptured the surface. Seismological and geodetic data show N–S crustal stretching and no evidence for the occurrence of a NE–SW-striking shear zone in the central part of Gökova Gulf.

The spatio-temporal evolution shows long quiescence of the main fault F1 and immediate generation with rapid evolution of aftershocks east of the epicentral area, also forming a hypocentral gap between the two. Aftershocks around the main fault occurred much later than the eastern cluster and with a slower rate concluding in an asymmetrical development of the two main clusters.

The post-sequence stress change suggests that (roughly) E–W-striking normal faults, located beyond the opposite tips (along strike) of both mainshock's and strongest aftershock's faults (F1 and F2, respectively), have been loaded with stresses, the eastern part of which was slightly relieved by the aftershock activity. As previously discussed, the western part lacks any 2017 aftershock activity. Moreover, diachronic seismicity (north of Pserimos Island, Fig. 1) and (known) faults also lack in the same area. Thus, this area is fully loaded with stress, but without any faults. Bodrum and Datça peninsulas lie within the stress-drop areas, implying a possible delay of future seismic activity.

References

Aki K (1966) Generation and propagation of G-waves from the Niigata earthquake of June 16, 1964. 2. Estimation of earthquake movement, released energy and stress-strain drop from G spectrum. Bull Earthq Res Inst 44:23–88

Aktar M, Karabulut H, Özalaybey S, Childs D (2007) A conjugate strike-slip fault system within the extensional tectonics of Western Turkey. Geophys J Int 171(3):1363–1375

Aktug B, Nocquet JM, Cingöz A, Parsons B, Erkan Y, England P, Tekgül A (2009) Deformation of western Turkey from a combination of permanent and campaign GPS data: limits to block-like behavior. J Geophys Res 114:B10404

Alcik H (2018) Investigation of local site responses at the Bodrum Peninsula (Southwest of Turkey) using the mainshock and aftershocks of the 20 July 2017 M_W 6.6 Bodrum–Kos earthquake. Ann Geophys 61(3):SE339

Altunel E, Stewart IS, Barka A, Piccardi L (2003) Earthquake faulting at ancient Cnidus, SW Turkey. Turkish J Earth Sci 12:137–151

Ambraseys NN, White D (1997) The seismicity of the eastern Mediterranean region 550–1 BC: a re-appraisal. J Earthq Eng 1(04):603–632

Benetatos C, Kiratzi A, Papazachos C, Karakaisis G (2004) Focal mechanisms of shallow and intermediate depth earthquakes along the Hellenic Arc. J Geodyn 37(2):253–296

Benetatos C, Kiratzi A, Ganas A, Ziazia M, Plessa A, Drakatos G (2006) Strike-slip motions in the Gulf of Siğaçik (western Turkey): properties of the 17 October 2005 earthquake seismic sequence. Tectonophysics 426(3–4):263–279

Cartwright JA, Trudgill BD, Mansfield CS (1995) Fault growth by segment linkage: an explanation for scatter in maximum displacement and trace length data from the Canyonlands Grabens of SE Utah. J Struct Geol 17(9):1319–1326

Chatzipetros A, Kiratzi A, Sboras S, Zouros N, Pavlides S (2013) Active faulting in the north-eastern Aegean Sea Islands. Tectonophysics 597:106–122

Cohen HA, Dart CJ, Akyüz HS, Barka A (1995) Syn-rift sedimentation and structural development of the Gediz and Büyük Menderes graben, western Turkey. J Geol Soc 152(4):629–638

Cowie PA, Scholz CH (1992) Physical explanation for the displacement-length relationship of faults using a post-yield fracture mechanics model. J Struct Geol 14(10):1133–1148

Dimova L, Raykova R (2018) Numerical simulations of the earthquake-induced tsunami of July 20, 2017 ($M_w = 6.6$) in Bodrum–Kos, Aegean Sea. Rev Bulg Geol Soc 79(1–2):5–12

Dogan GG, Annunziato A, Papadopoulos GA, Guler HG, Yalciner AC, Cakir TE, Guler I (2019) The 20th July 2017 Bodrum–Kos Tsunami Field Survey. Pure appl Geophys 176(7):2925–2949

Duman TY, Emre Ö, Özalp S, Elmaci H (2011) Active fault map series of Turkey, Aydin (NJ35-11) Quadrangle. Serial Number: 7, General Directorate of Mineral Research and Exploration, Ankara, Turkey

Elitez İ, Yaltırak C, Aktuğ B (2016) Extensional and compressional regime driven left-lateral shear in southwestern Anatolia (eastern Mediterranean): the Burdur–Fethiye Shear Zone. Tectonophysics 688:26–35

Emre Ö, Duman TY, Özalp S (2011) Active fault map series of Turkey, Marmaris (NJ35-15) Quadrangle. Serial Number: 8, General Directorate of Mineral Research and Exploration, Ankara, Turkey

England P, Houseman G, Nocquet JM (2016) Constraints from GPS measurements on the dynamics of deformation in Anatolia and the Aegean. J Geophys Res Solid Earth 121(12):8888–8916

Font Y, Kao H, Lallemand S, Liu C-S, Chiao L-Y (2004) Hypocentral determination off-shore Eastern Taiwan using the maximum intersection method. Geophys J Int 158:655–675

Ganas A, Elias P, Kapetanidis V, Valkaniotis S, Briole P, Kassaras I, Argyrakis P, Barberopoulou A, Moshou A (2019) The July 20, 2017 M 6.6 Kos earthquake: seismic and geodetic evidence for an active north-dipping normal fault at the western end of the Gulf of Gökova (SE Aegean Sea). Pure Appl Geophys 176(10):4177–4211

Gupta A, Scholz CH (2000) A model of normal fault interaction based on observations and theory. J Struct Geol 22(7):865–879

Gürer ÖF, Yilmaz Y (2002) Geology of the Ören and surrounding areas, SW Anatolia. Turk J Earth Sci 11(1):1–13

Gürer ÖF, Sarica-Filoreau N, Özburan M, Sangu E, Doğan B (2009) Progressive development of the Büyük Menderes Graben based on new data, western Turkey. Geol Mag 146(5):652–673

Hall J, Aksu AE, Elitez I, Yaltırak C, Çifçi G (2014) The Fethiye–Burdur Fault Zone: a component of upper plate extension of the subduction transform edge propagator fault linking Hellenic and Cyprus Arcs, Eastern Mediterranean. Tectonophysics 635:80–99

Hancock PL, Barka AA (1987) Kinematic indicators on active normal faults in western Turkey. J Struct Geol 9(5–6):573–584

Harris RA (1998) Introduction to special section: stress triggers, stress shadows, and implications for seismic hazard. J Geophys Res 103(B10):24347–24358

Hatzfeld D (1999) The present-day tectonics of the Aegean as deduced from seismicity. Geol Soc Lond Spec Publ 156(1):415–426

Heidarzadeh M, Necmioglu O, Ishibe T, Yalciner AC (2017) Bodrum–Kos (Turkey–Greece) M_W 6.6 earthquake and tsunami of 20 July 2017: a test for the Mediterranean tsunami warning system. Geosci Lett 4(1):31

Hollenstein C, Müller MD, Geiger A, Kahle HG (2008) Crustal motion and deformation in Greece from a decade of GPS measurements, 1993–2003. Tectonophysics 449(1–4):17–40

Institute of Engineering Seismology and Earthquake Engineering (IESEE) (2017) Earthquake of Kos M_W 6.6 on 21 July 2017: Preliminary Report, Thessaloniki, p 20

Institute of Geology and Mineral Exploration (IGME) (1998) Geological map of Greece, "Eastern Kos" sheet, 1:50,000, Athens, Greece

İşcan Y, Tur H, Gökaşan E (2013) Morphologic and seismic features of the Gulf of Gökova, SW Anatolia: evidence of strike-slip faulting with compression in the Aegean extensional regime. Geo Mar Lett 33(1):31–48

Jenny S, Goes S, Giardini D, Kahle HG (2004) Earthquake recurrence parameters from seismic and geodetic strain rates in the eastern Mediterranean. Geophys J Int 157(3):1331–1347

Karasözen E, Nissen E, Büyükakpınar P, Cambaz MD, Kahraman M, Kalkan Ertan E, Abgarmi B, Bergman E, Ghods A, Özacar AA (2018) The 2017 July 20 M_w 6.6 Bodrum–Kos earthquake illuminates active faulting in the Gulf of Gökova, SW Turkey. Geophys J Int 214(1):185–199

Kiratzi A, Koskosidi A (2018) Constrains on the near-source motions of the Kos–Bodrum 20 July 2017 M_W 6.6 earthquake. In: 16th European conference on earthquake engineering, June 18–21, 2018, Thessaloniki, Greece, pp 18–21

Kiratzi A, Louvari E (2003) Focal mechanisms of shallow earthquakes in the Aegean Sea and the surrounding lands determined by waveform modelling: a new database. J Geodyn 36(1–2):251–274

King GCP, Cocco M (2001) Fault interaction by elastic stress changes: new clues from earthquake sequences. Adv Geophys. https://doi.org/10.1016/S0065-2687(00)80006-0

Konca AO, Guvercin SE, Ozarpaci S, Ozdemir A, Funning GJ, Dogan U, Ergintav S, Floyd M, Karabulut H, Reilinger R (2019) Slip distribution of the 2017 M_w 6.6 Bodrum–Kos earthquake: resolving the ambiguity of fault geometry. Geophys J Int 219(2):911–923

Kurt H, Demirbağ E, Kuşçu İ (1999) Investigation of the submarine active tectonism in the Gulf of Gökova, southwest Anatolia–southeast Aegean Sea, by multi-channel seismic reflection data. Tectonophysics 305(4):477–496

Lomax A, Curtis A (2001) Fast, probabilistic earthquake location in 3D models using oct-tree importance sampling. European Geophysical Society, Nice

Lomax A, Virieux J, Volant P, Berge C (2000) Probabilistic earthquake location in 3D and Layered models: introduction of a Metropolis–Gibbs method and comparison with linear locations. In: Thurber CH, Rabinowitz N (eds) Advances in seismic event location. Kluwer, Amsterdam, pp 101–134

Mascle J, Martin L (1990) Shallow structure and recent evolution of the Aegean Sea: a synthesis based on continuous reflection profiles. Mar Geol 94(4):271–299

Nocquet JM (2012) Present-day kinematics of the Mediterranean: a comprehensive overview of GPS results. Tectonophysics 579:220–242

Nomikou P, Papanikolaou D (2010) The morpho-tectonic structure of Kos–Nisyros–Tilos volcanic area based on onshore and offshore data. In: Proceedings of the XIX CBGA congress, Thessaloniki, Greece, Special volume 99, pp 557–564

Nomikou P, Papanikolaou D, Dietrich VJ (2018) Geodynamics and volcanism in the Kos–Yali–Nisyros volcanic field. In: Dietrich VJ, Lagios E (eds) Nisyros volcano–active volcanoes of the World. Springer, Cham, pp 13–55

Ocakoğlu N (2012) Investigation of Fethiye–Marmaris Bay (SW Anatolia): seismic and morphologic evidences from the missing link between the Pliny Trench and the Fethiye–Burdur Fault Zone. Geo Mar Lett 32(1):17–28

Ocakoğlu N, Nomikou P, İşcan Y, Loreto MF, Lampridou D (2018) Evidence of extensional and strike-slip deformation in the offshore Gökova–Kos area affected by the July 2017 M_W 6.6 Bodrum–Kos earthquake, eastern Aegean Sea. Geo Mar Lett 38(3):211–225

Okada Y (1992) Internal deformation due to shear and tensile faults in a half-space. Bull Seismol Soc Am 82(2):1018–1040

Panagiotopoulos DG, Hatzidimitriou PM, Karakaisis GF, Papadimitriou EE, Papazachos BC (1985) Travel time residuals in southeastern Europe. Pure Appl Geophys 123:221–231

Papathanassiou G, Valkaniotis S, Pavlides S (2019) The July 20, 2017 Bodrum–Kos, Aegean Sea M_W 6.6 earthquake; preliminary field observations and image-based survey on a lateral spreading site. Soil Dyn Earthq Eng 116:668–680

Papazachos B, Papazachou C (2003) The earthquakes of Greece. Ziti Editions, Thessaloniki

Pe-Piper G, Piper DJ, Perissoratis C (2005) Neotectonics and the Kos Plateau Tuff eruption of 161 ka, South Aegean arc. J Volcanol Geoth Res 139(3–4):315–338

Psycharis IN, Taflampas IM (2017) Preliminary evaluation of ground motion in Kos town during the 21 July 2017 earthquake. Report published online https://psycharis.weebly.com/uploads/1/6/2/5/16258088/kos.pdf **(in Greek)**

Reilinger R, McClusky S, Vernant P, Lawrence S, Ergintav S, Cakmak R et al (2006) GPS constraints on continental deformation in the Africa–Arabia–Eurasia continental collision zone and implications for the dynamics of plate interactions. J Geophys Res 111:B05411

Reilinger R, McClusky S, Paradissis D, Ergintav S, Vernant P (2010) Geodetic constraints on the tectonic evolution of the Aegean region and strain accumulation along the Hellenic subduction zone. Tectonophysics 488(1–4):22–30

Ring U, Gessner K, Thomson S (2017) Variations in fault-slip data and cooling history reveal corridor of heterogeneous backarc extension in the eastern Aegean Sea region. Tectonophysics 700:108–130

Rontogianni S, Konstantinou KI, Evangelidis C, Melis NS (2011) Investigating potential Seismic Hazard in the Gulf of Gökova (South Eastern Aegean Sea) deduced from recent shallow earthquake activity. American Geophysical Union, Fall Meeting 2011, T43E-2427, San Francisco, USA

Sakellariou D, Tsampouraki-Kraounaki K (2019) Plio-Quaternary extension and strike-slip tectonics in the Aegean. In: Transform plate boundaries and fracture zones, Elsevier. Elsevier, pp 339–374

Saltogianni V, Taymaz T, Yolsal-Çevikbilen S, Eken T, Gianniou M, Öcalan T, Pytharouli S, Stiros S (2017) Fault-model of the 2017 Kos–Bodrum (east Aegean Sea) M_W 6.6 earthquake from inversion of seismological and GPS data—preliminary report. Report published online on www.emsc-csem.org

Sboras S, Lazos I, Mouzakiotis E, Karastathis V, Pavlides S, Chatzipetros A (2018) Epicentral relocation, fault modelling, static stress change distribution and modelled surficial displacements of the July 20, 2017 (M_W 6.6) Kos–Bodrum earthquake sequence. In: 9th international INQUA meeting on paleoseismology, active tectonics and archeoseismology (PATA), 25–27 June 2018, Possidi, Greece, pp 247–250

Stein RS (1999) The role of stress transfer in earthquake occurrence. Nature 402(6762):605

Taymaz T, Price S (1992) The 1971 May 12 Burdur earthquake sequence, SW Turkey: a synthesis of seismological and geological observations. Geophys J Int 108(2):589–603

ten Veen JH (2004) Extension of Hellenic forearc shear zones in SW Turkey: the Pliocene–Quaternary deformation of the Eşen Çay Basin. J Geodyn 37(2):181–204

Tiryakioğlu İ, Aktuğ B, Yiğit CÖ, Yavaşoğlu HH, Sözbilir H, Özkaymak Ç, Özener H (2018) Slip distribution and source parameters of the 20 July 2017 Bodrum–Kos earthquake (M_W 6.6) from GPS observations. Geodin Acta 30(1):1–14

Toda S, Stein RS, Sagiya T (2002) Evidence from the AD 2000 Izu islands earthquake swarm that stressing rate governs seismicity. Nature 419(6902):58–61

Toda S, Stein RS, Beroza GC, Marsan D (2012) Aftershocks halted by static stress shadows. Nat Geosci 5(6):410–413

Tsampouraki-Kraounaki K, Sakellariou D (2017) Strike-slip deformation behind the Hellenic subduction: the Amorgos Shear Zone, South Aegean Sea. In: Proceedings of the 8th international INQUA meeting on paleoseismology, active tectonics and archeoseismology, pp 392–395

Tur H, Yaltırak C, Elitez İ, Sarıkavak KT (2015) Pliocene-Quaternary tectonic evolution of the Gulf of Gökova, southwest Turkey. Tectonophysics 638:158–176

Uluğ A, Duman M, Ersoy Ş, Özel E, Avcı M (2005) Late Quaternary sea-level change, sedimentation and neotectonics of the Gulf of Gökova: southeastern Aegean Sea. Mar Geol 221(1–4):381–395

Vernant P, Reilinger R, McClusky S (2014) Geodetic evidence for low coupling on the Hellenic subduction plate interface. Earth Planet Sci Lett 385:122–129

Wells DL, Coppersmith JK (1994) New empirical relationships among magnitude, rupture length, rupture width, rupture area, and surface displacement. Bull Seismol Soc Am 84:974–1002

Yalçıner AC, Annunziato A, Papadopoulos G, Dogan GG, Guler HG, Cakir TE, Sozdinler CO, et al (2017) The 20th July 2017 (22:31 UTC) Bodrum/Kos earthquake and tsunami: post tsunami field survey report. Report published online on www.emsc-csem.org

Yilmaz Y, Genç ŞC, Gürer F, Bozcu M, Yilmaz K, Karacik Z, Altunkaynak Ş, Elmas A (2000) When did the western Anatolian grabens begin to develop? Geol Soc Lond Spec Publ 173(1):353–384

Yolsal-Cevikbilen S, Taymaz T, Helvacı C (2014) Earthquake mechanisms in the Gulfs of Gökova, Sığacık, Kuşadası, and the Simav Region (western Turkey): neotectonics, seismotectonics and geodynamic implications. Tectonophysics 635:100–124

Zanchi A, Angelier J (1993) Seismotectonics of western Anatolia: regional stress orientation from geophysical and geological data. Tectonophysics. https://doi.org/10.1016/0040-1951(93)90052-L